communications earth & environment

Article

https://doi.org/10.1038/s43247-024-01746-4

Marine clay maturation induces systematic silicon isotope decrease in authigenic clays and pore fluids

Sonja Geilert [1,2] ✉, Daniel A. Frick [3,4], April N. Abbott [5] & Stefan C. Löhr [6,7]

Marine silicate alteration exerts a major influence on marine carbon and cation cycles, but has proven difficult to quantify. In this context, silicon isotopes of marine pore fluids became an important tracer. However, poorly constrained silicon isotope signatures of precipitates produced during silicate alteration (i.e. authigenic clays) remain a major source of uncertainty. Here we present in situ silicon isotope analyses of marine authigenic clays (intergrown iron-smectites and iron-glauconites) occurring within recent sediments from the Oregon margin, eastern North Pacific. We identify a trend to lower silicon isotopes (from −2.24‰ to −3.17‰), accompanied by decreasing aluminum/silicon ratios and increasing potassium oxide contents, which we interpret as an isotopic shift caused by progressive clay maturation via dissolution-reprecipitation reactions. Our modelling suggests that this clay maturation pathway, together with mixing of other fluid sources, may induce pore fluid silicon isotope shifts of up to −1.7‰, if sufficient newly precipitated clays are re-dissolved. This could potentially produce silicon isotopes values significantly lower than seawater and implies that conventional isotope-based approaches underestimate the prevalence of marine silicate alteration. Our findings highlight that clay maturation must be considered when interpreting silicon isotope signatures in terms of marine silicate alteration and upscaling to global element cycles.

Marine silicate alteration (MSA), the dissolution and precipitation of silicate minerals, is a key control on marine carbon and cation budgets[1–5]. MSA is divided into forward weathering, which is the dissolution of detrital minerals, releasing cations and alkalinity and consuming CO_2; and reverse weathering, which is the formation of authigenic clays (e.g. smectite, glauconite), consuming cations and alkalinity and releasing CO_2[1,4,6,7]. The first authigenic precipitates are often Si-Al gels[8]. These gels can transform to smectites and further to glauconites in organic-rich sediments under reducing conditions in confined microenvironments, taking up K^+ and Mg^{2+} from seawater/pore fluids, metals from dissolving metal-oxides, and Si from dissolving biogenic silica and detrital minerals, while releasing H^+[6,7]. Despite the importance of MSA and its first description decades ago[9], MSA remains difficult to identify and quantify, and this is mainly attempted indirectly via shifts in pore fluid composition[1,10,11]. MSA can consume up to 5-20 Tmol CO_2 per year[1], similar or even in excess of terrestrial CO_2 consumption rates (11 – 23 Tmol per year)[12,13], however the marine data set is comparatively small. The net effect of MSA is highly uncertain because counteracting processes that release CO_2, such as marine authigenic clay formation, can occur simultaneously[14]. Unknown reaction rates and CO_2 budgets create large uncertainties in global carbon and climate models[4,15]. Our lack of understanding of MSA processes causes a large knowledge gap in reconstructing the chemical composition of the ocean in the geological past, impacting our ability to forecast global CO_2 and cation turnover, and even hampering the application of CO_2-removal strategies to mitigate global climate change.

In recent years, silicon isotopes ($\delta^{30}Si$) have been the most widely used tracer in detecting MSA, given that distinct isotopic signatures in marine pore fluids can be related to silicate dissolution and authigenic clay precipitation. From the Si released during silicate dissolution, the light Si isotopes are preferentially taken up in the solid phase during (consecutive) precipitation[11,16–19]. An important process during MSA is the formation of secondary authigenic clays, which can shift pore fluid $\delta^{30}Si$ to high values,

[1]Department of Earth Sciences, Utrecht University, Princetonplein 9, 3584 CC Utrecht, the Netherlands. [2]GEOMAR Helmholtz Centre for Ocean Research Kiel, Wischhofstr. 1-3, 24148 Kiel, Germany. [3]GFZ German Research Centre for Geosciences, 14473 Potsdam, Germany. [4]Institute of Geosciences, Kiel University, Ludewig-Meyn-Str. 10, 24118 Kiel, Germany. [5]Department of Marine Science, Coastal Carolina University, Conway, SC, 29526, USA. [6]School of Physics, Chemistry and Earth Sciences, University of Adelaide, Adelaide, 5005 SA, Australia. [7]School of Natural Sciences, Macquarie University, Sydney, 2109, Australia. ✉e-mail: s.geilert@uu.nl

often exceeding seawater values[16]. Therefore, high pore fluid $\delta^{30}Si$ is often used as evidence for authigenic clay formation, without further consideration of the nature of these precipitates. This generalization bears certain risks as a large range of marine authigenic clay types exist, showing broad compositional range[6,7,20,21] and thus likely also distinct Si isotope signatures. However, authigenic clays are difficult to characterise due to their small size (typically µm to sub-µm) and their intermingled occurrence with detrital clays[22]. Consequently, current constraints on authigenic clay $\delta^{30}Si$ signatures derive from sequential leaching methods[23,24], which always bear the risk of unwanted co-dissolving mineral phases (e.g. detrital clays), obscuring target mineral Si isotope signatures. The large uncertainties associated with these $\delta^{30}Si$ signatures consequently also transfers to inferred benthic fluxes, alkalinity, and cation budgets.

In this study, we use a new approach to identify the $\delta^{30}Si$ signature of authigenic clays by measuring in situ on a µm-scale Si isotopes in Fe-smectites and Fe-glauconites from the Oregon margin (North Pacific). These clays have formed pellets 100 s of µm in size, clearly separated from the detrital clays that comprise the remaining sediment, and have recently been mineralogically characterized[20,25]. This well-characterized sample set allows us to probe the extent to which Si isotope fractionation depends on the clay type and to investigate if and how they evolve during authigenic clay maturation. Our Si isotope results show a large range in $\delta^{30}Si$ spanning ~1‰, with a systematic shift to lower values with increasing clay maturity. Our study highlights that pore fluid $\delta^{30}Si$ has to be interpreted with care with respect to silicate alteration, taking into consideration clay type, maturation states, and formation processes.

Results

Authigenic clay geochemistry and types

X-ray diffraction analysis of the Oregon margin sediments (sample HH1200-1 from 0 to 1.2 cm and HH1200-6 from 6.2 to 7.4 cm sediment depth) has identified a chemically immature mineral assemblage consisting of detrital quartz, feldspar (primarily albite), chlorite, mica (muscovite and/or illite), pyroxenes, amphibole, and biogenic silica, as well as authigenic clays (Fe-smectite and glauconite)[20,25]. The distinction between detrital and authigenic clays is based on their morphology, as detrital clays have discrete grain boundaries and angular shapes that stand in contrast to authigenic clays, which are curvy, concentrated in pore-filling domains, and grow around detrital grains[22] (Fig. 1). Authigenic clays are concentrated within sand-sized pellets (up to 1500 µm) formed via early diagenetic alteration of macrofaunal fecal pellets close to the sediment-water interface, where they cement and (partially) replace the primary detrital and biogenic constituents (Fig. 1). SEM imaging identifies textural maturities ranging from fragile, incompletely cemented incipient pellets containing a high abundance of detrital components (e.g. HH1200-6 ROI-3), to fully formed mature clay pellets containing a lower quantity of detrital inclusions (e.g. HH1200-6 ROI-4). The latter, well-cemented, authigenic-clay dominated pellets were targeted for in situ Si isotope analyses.

Electron Microprobe (EMP) analyses confirm that the authigenic clays formed at the Oregon margin are comprised of intergrown Fe-smectite and more mature Fe-rich glauconite, with average (± 1 SD) SiO_2, Fe_2O_3, K_2O, and Al_2O_3 contents of 55.4 ± 0.9, 31.9 ± 2.5, 4.0 ± 0.8, and 2.6 ± 2.0 wt%, respectively (Fig. 2; Table 1; individual analyses shown in Supplementary Table 1). Authigenic clay K_2O and Fe_2O_3 are positively correlated, but are negatively correlated with Al_2O_3 and SiO_2 (Fig. 2), indicating that maturation of Fe-smectite to glauconite has proceeded through the substitution of Fe^{3+} and Fe^{2+} for Al^{3+} in the octahedral sites and of Al^{3+} and Fe^{3+} for Si^{4+} in the tetrahedral sites, with uptake of K^+ in glauconite interlayer sites required for charge balance[6]. This mineralogical evolution is also evident in a cross-plot of $M^+*(Si/4)^{-1}$ versus $^{VI}Fe_{total}/\Sigma^{VI}$, in which M^+ represents the sum of the interlayer charge (Na + K + 2Ca), Si/4 is the amount of tetrahedral Si and $^{VI}Fe_{total}/\Sigma^{VI}$ is the structural iron divided by the sum of octahedral bound cations, which are $^{VI}Fe^{2+/3+}$, $^{VI}Mg^{2+}$, and $^{VI}Al^{3+}$ following Baldermann et al.[6] and Meunier & El Albani[26] (Fig. 2a). The samples show no mineralogical or geochemical distinction between the two sampling depths.

Authigenic clay Si isotope signatures

In situ $\delta^{30}Si$ measurements on authigenic clays range from −2.13‰ (1200-6 ROI 4 B1) to −3.17‰ (1200-6 ROI 4 A2) (Figs. 1, 3; Table 1). The Al/Si mass ratios range between 0.02 and 0.16, excluding sample 1200-1 ROI 2 A1, which has a higher ratio of 0.54, which we attribute to unintended ablation of detrital silicate grains. A positive correlation is observed between $\delta^{30}Si$ and Al/Si (Fig. 3a). Excluding sample 1200-1 ROI 2, where detrital material was likely ablated, the $\delta^{30}Si$ range within a single clay pellet mineral is ≤ 0.52‰

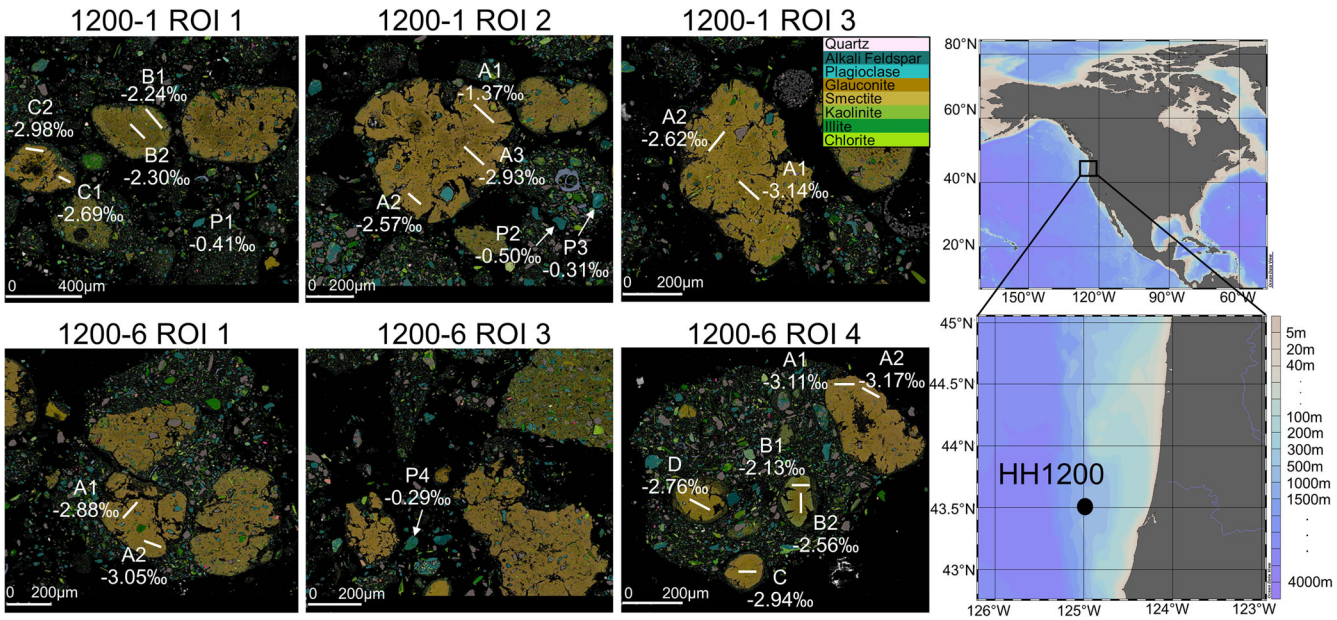

Fig. 1 | Site location off the Oregon margin and mineral maps of selected samples. Map showing the sampling location of core HH1200 (map created in Ocean Data View, odv.awi.de, Schlitzer, R., 2023). Individual mineral maps of the 6 investigated regions of interest (ROI) as well as areas (white lines) and results of in situ $\delta^{30}Si$ in clays (labelled A to D) and plagioclase (labelled P1 to P4). Only texturally mature (well-cemented) glauconite/smectite phases were chosen for Si isotope analyses.

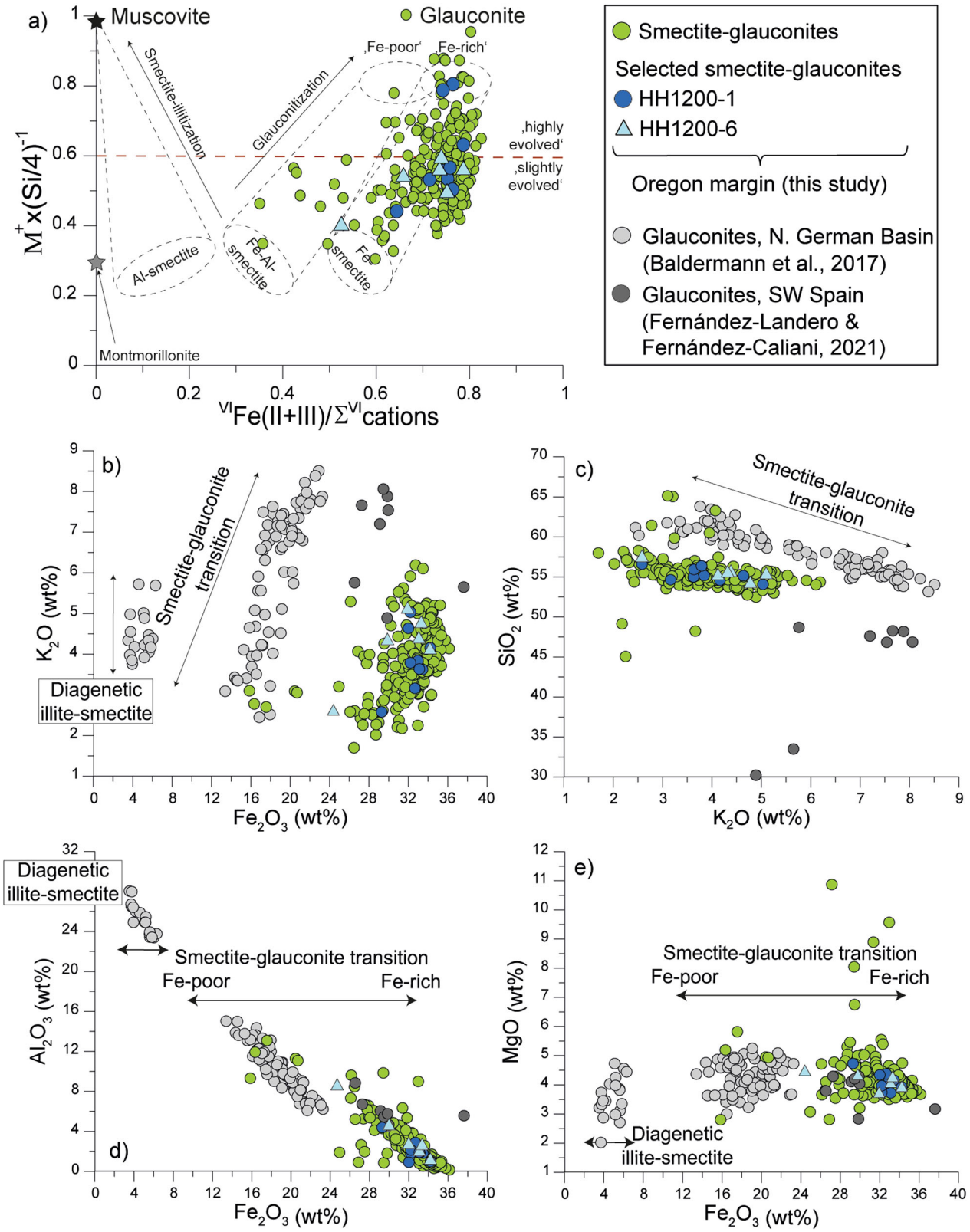

Fig. 2 | Geochemical characterization of authigenic clays at the Oregon margin. **a** Glauconitization process modified after Baldermann et al.[6] and Meunier and Albani[26]. **b**–**e** Cross-plots of K_2O, Fe_2O_3, Al_2O_3, MgO and SiO_2. Selected smectite-glauconites indicate the samples further processed for $\delta^{30}Si$ analyses. For comparison, smectite-glauconites from the Northern German Basin[6] and from SW Spain[28] are shown.

Table 1 | Geochemical characterisation of Oregon margin samples

Sample	n[a]	SiO_2 (wt%)	Fe_2O_3 (wt%)	MgO (wt%)	K_2O (wt%)	Al_2O_3 (wt%)	CaO (wt%)	Na_2O (wt%)	$\delta^{30}Si$ (‰)	2SE (‰)	$\delta^{29}Si$ (‰)	2SE (‰)	Al/Si mass ratio[c]
Smectite-Glauconites													
Depth interval 0–1.2 cm below seafloor													
1200-1 ROI1 B1	8	56.6	29.3	4.7	2.6	4.4	0.6	0.9	−2.24	0.09	−1.19	0.07	0.10
1200-1 ROI1 B2	6	54.6	32.7	4.4	3.2	2.9	0.7	0.9	−2.30	0.14	−1.25	0.09	0.08
1200-1 ROI1 C1	6	55.9	33.1	3.7	3.6	1.9	0.1	1.1	−2.69	0.12	−1.40	0.08	0.03
1200-1 ROI1 C2	5	56.4	32.2	3.7	3.8	1.8	0.5	1.0	−2.98	0.08	−1.54	0.07	0.04
1200-1 ROI2 A1[b]	6	55.2	33.0	4.2	3.8	1.9	0.4	0.9	−1.37	0.23	−0.60	0.14	0.54
1200-1 ROI2 A2	10	55.0	33.4	4.2	3.6	1.8	0.4	1.0	−2.57	0.10	−1.33	0.07	0.09
1200-1 ROI2 A3	9	54.6	34.2	3.9	4.2	1.0	0.5	1.1	−2.93	0.06	−1.52	0.05	0.04
1200-1 ROI3 A1	6	55.2	32.0	4.3	4.6	0.9	1.0	1.5	−3.14	0.08	−1.51	0.06	0.03
1200-1 ROI3 A2	5	54.1	32.2	4.0	5.0	2.1	0.6	1.5	−2.62	0.17	−1.33	0.12	0.04
Depth interval 6.2–7.4 cm below seafloor													
1200-6 ROI1 A1	3	55.6	33.1	4.0	4.4	1.9	0.4	0.2	−2.88	0.08	−1.50	0.06	0.04
1200-6 ROI1 A2	3	54.1	33.3	4.2	4.8	2.5	0.5	0.2	−3.05	0.09	−1.61	0.07	0.04
1200-6 ROI4 A1	9	55.2	34.2	3.9	4.1	1.0	0.4	0.9	−3.11	0.08	−1.66	0.06	0.02
1200-6 ROI4 A2									−3.17	0.09	−1.65	0.06	0.02
1200-6 ROI4 B1	9	57.4	24.5	4.5	2.6	8.6	0.8	0.4	−2.13	0.08	−1.13	0.06	0.16
1200-6 ROI4 B2									−2.56	0.07	−1.36	0.06	0.10
1200-6 ROI4 C	6	55.3	32.0	3.7	5.1	2.5	0.3	0.5	−2.94	0.07	−1.51	0.06	0.04
1200-6 ROI4 D	6	55.5	29.8	4.3	4.3	4.5	0.6	0.4	−2.76	0.07	−1.42	0.05	0.07
Feldspars/ Plagioclase													
1200-1 ROI1 P1	8	63.3	1.3	0.8	0.2	20.8	4.3	10.9	−0.41	0.10	−0.23	0.08	0.38
1200−1 ROI2 P2	10	67.0	0.7	1.4	1.8	19.7	0.5	10.3	−0.50	0.12	−0.31	0.10	0.35
1200−1 ROI2 P3	7	65.3	2.5	7.7	0.7	16.2	0.4	8.9	−0.63	0.13	−0.27	0.09	0.30
1200-6 ROI3 P4	11	65.9	1.0	0.5	4.6	19.8	1.2	6.9	−0.29	0.11	−0.15	0.07	0.37

Average geochemical (EMP) and Si isotope (fsLA-MC-ICP-MS) analyses of Oregon margin smectite-glauconites and feldspars
Grey/white marking indicates individual minerals.
[a]Number of analyses.
[b]Mixture analysis of a detrital phase and an authigenic clay.
[c]Based on MC-ICPMS measurements.

and thus relatively homogeneous considering the large total range. Cross-plots of $\delta^{30}Si$ versus major cations show distinct correlations, with decreasing $\delta^{30}Si$ with increasing K_2O and Fe_2O_3 contents and decreasing Al_2O_3 contents (Fig. 3). There is no isotopic difference between the two sampling depths.

Plagioclase samples yield $\delta^{30}Si$ between −0.29‰ and −0.63‰, similar to previously reported plagioclase (albite) values (−0.4‰[27]). Plagioclase Al/Si ratios range between 0.30 and 0.38 (Figs. 1, 3; Table 1).

Discussion

The impact of clay maturation on Si isotopes

Authigenic clays can undergo substantial compositional and mineralogical change during early diagenesis, evolving from disordered, reactive initial precipitates to increasingly ordered, mature clays such as glauconite[6]. K^+ content is a robust maturity indicator for the smectite to glauconite series, since K^+ uptake to the interlayer sites is required to maintain charge balance with progressive glauconitization[21,28–30]. We can therefore link the systematic decrease in $\delta^{30}Si$ along with decreasing SiO_2 and increasing K_2O concentrations (Fig. 3) to increasing authigenic clay maturation, whereby the light Si isotopes are preferentially incorporated from solution.

A similar trend to lower $\delta^{30}Si$ with increasing weathering degree was also found in terrestrial river sediments[31], a paleo-delta[32] and a marine shelf[16] (total range from +0.33‰ to −2.16‰) here, however, increasing Al/Si ratios, indicate different mineralogical pathways during clay formation.

Also during opal maturation in a geothermal setting, a $\delta^{30}Si$ shift of −1‰ has been attributed to repetitive dissolution-reprecipitation reactions, continuously favouring the light Si isotope in the precipitate[33]. We propose that a similar recrystallisation process can explain the isotopic shift from less mature, relatively K-poor Fe-smectite to a more mature, K-rich glauconite product[30], where in each dissolution-reprecipitation step the light isotopes are favoured in the more mature precipitate (Figs. 3, 4).

The fate of $\delta^{30}Si$: a reliable silicate alteration tracer in pore fluids?

Authigenic clay formation involves the preferential uptake of light Si isotopes, so that shifts in pore fluid $\delta^{30}Si$ to values higher than seawater or biogenic silica signatures are widely interpreted as evidence for authigenic clay formation[11,16–19,34]. While this general inference is in most cases likely correct, any quantitative assessment of silicate alteration rates and benthic fluxes is hampered by the scarcity of direct authigenic clay $\delta^{30}Si$ measurements. Consequently, the extent to which clay $\delta^{30}Si$ varies as a function of clay type and clay maturity, and how this affects pore fluid $\delta^{30}Si$, remains largely unknown.

In order to investigate the impact of early clay diagenesis on the pore fluid $\delta^{30}Si$ tracer, we construct a simple Rayleigh model that incorporates repeated dissolution and reprecipitation steps. Next to clay diagenesis, Oregon margin pore fluids are influenced by dissolution of biogenic silica (diatoms) and detrital minerals[20]. As we do not know the Si fractionation factor between fluid and solid, $\delta^{30}Si$ of diatoms, ambient seawater and pore

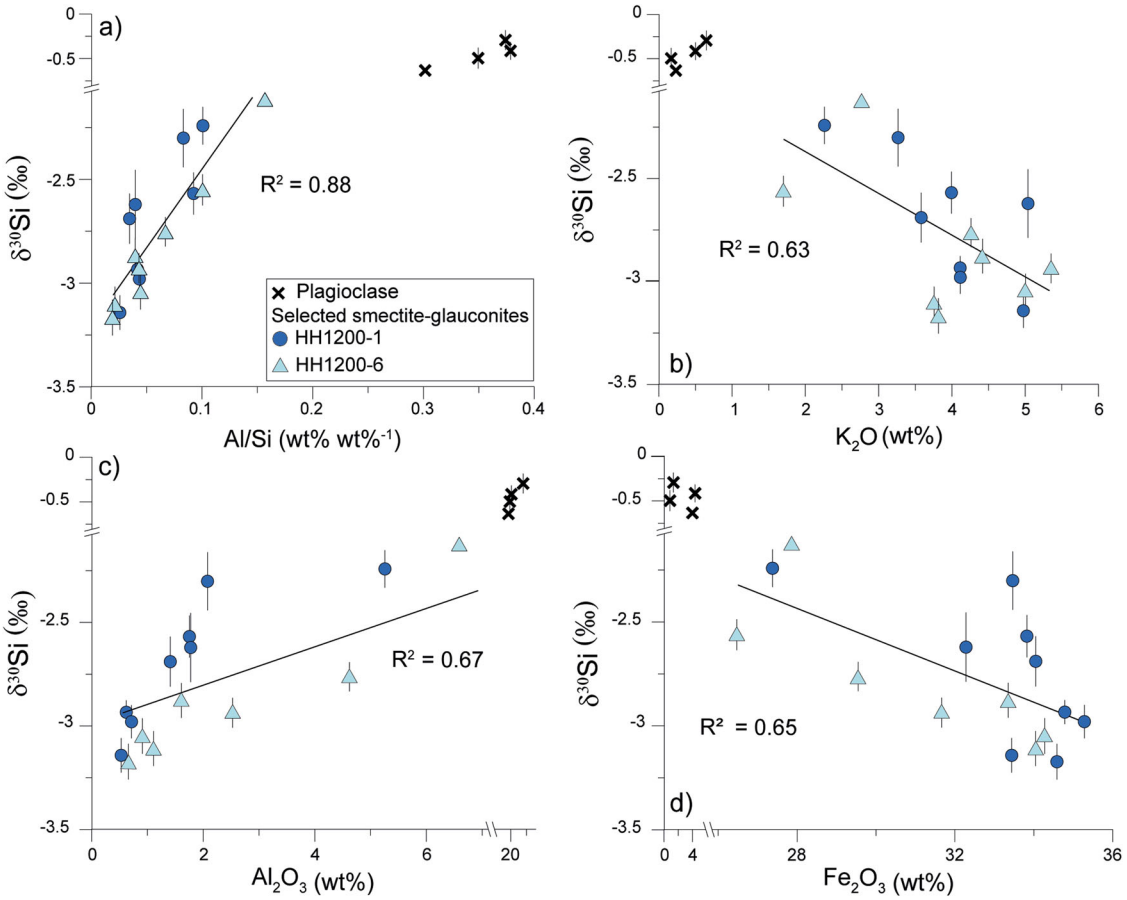

Fig. 3 | Isotopic and geochemical variations in Oregon margin samples. In situ Si isotopes in authigenic smectite-glauconites and plagioclase shown as $\delta^{30}Si$ versus the (**a**) Al/Si ratio, (**b**) K_2O, (**c**) Al_2O_3, and (**d**) Fe_2O_3. Error bars are 2 SE.

fluids or the amount of the respective fluid fraction that reprecipitates, we need to make reasonable assumptions to constrain our model (see Supplementary Method 1 and Supplementary Table 2). An alternative model, with a different starting solution taking a lower diatom $\delta^{30}Si$ value into account is discussed in the supplementary information 1. We emphasize that our model aims to explore the potential magnitude of the pore fluid $\delta^{30}Si$ shift associated with authigenic clay maturation, not model real pore fluid values for the Oregon margin.

The best fits with the measured smectite-glauconite data are obtained with a fractionation between pore fluid and authigenic clay of −3‰ after 5 dissolution-reprecipitation steps (Fig. 4, Supplementary Fig. 1; Supplementary Table 2). The model with 5 repetitive steps is discussed in detail below. After initial mixing of dissolving diatoms, detrital minerals (albite, smectite), and seawater, an immature amorphous silica-gel phase likely precipitates in dependence of the silica saturation state[29], with a modelled $\delta^{30}Si$ of −1.3‰. This fits well with Si isotope analyses of a poorly crystalline, immature authigenic clay phase from the Peruvian margin[16] and authigenic silica from the Gulf of Mexico[23] (Fig. 4). The corresponding modelled pore fluid phase becomes isotopically heavier, shifting to values higher than corresponding seawater (1.7‰ and 1.25‰[35], respectively), fitting well with the current criteria for identifying authigenic clay precipitation. Subsequently, mixing of other sources with low $\delta^{30}Si$ values and repetitive dissolution and reprecipitation processes shift pore fluid $\delta^{30}Si$ to values lower than seawater (from 1.1‰ to 0.1‰), as the light Si isotopes are consecutively enriched in the fluid phase. This is particular true if dissolution dominates over precipitation (only 20% of the dissolved Si re-precipitates as authigenic clay; see supplementary method 1 for details), which is however difficult to constrain in the current work. The dissolution of detrital phases, especially clay, is enhanced by the degradation of organic matter that lowers pore fluid pH[6,36]. The newly formed authigenic clay (here Fe-smectite) is thermodynamically unstable during early diagenesis[8], dissolves completely, and transforms to the more stable glauconite phase[6,28]. In total, 5 dissolution-reprecipitation steps are required to approach the lowest $\delta^{30}Si$ values measured in the authigenic clays. A pore fluid $\delta^{30}Si$ shift of up to -1.7‰ was achieved in our model (Fig. 4; Supplementary Table 2). These inferred multiple fractionation steps are also identified in leaching experiments investigating different Si pools in marine sediments, even summing up to a $\delta^{30}Si$ difference of −5‰[23].

It is also important to note that all model approaches reach similar pore fluid results after fractionation step 1 (a difference in $\delta^{30}Si < 0.2$‰), when clay maturation dominates and determines the fluid composition. This finding also highlights, that the importance of the starting seawater and diatom Si isotopic composition decreases with increasing clay maturation (Supplementary Table 2).

Si isotopes in marine pore fluids: implications for tracer applicability

According to the K_2O-based maturation classification of Odin and Matter[30], the Oregon glauconites are in the early or nascent stage (≤ 1000 yrs). Taking the lowest sedimentation rate of 0.5 mm yr^{-1} measured at the Oregon shelf in ~200 m depth[37] as a maximum rate gives minimum ages of 12 to 136 years for the average depth at HH1200-1 and HH1200-6, respectively. The large Si isotope shift in the solids ($\Delta^{30}Si_{glauconite\text{-}smectite} = -0.99$‰) and the overall modelled pore fluid shift ($\Delta^{30}Si_{modelled} = -1.7$‰) introduced already during this nascent clay maturation stage and well before 1000 years, will significantly hamper interpretations of pore fluid $\delta^{30}Si$ with respect to reverse weathering and silicate alteration in general. Whether further clay maturation produces an even larger fractionation is currently unknown, but

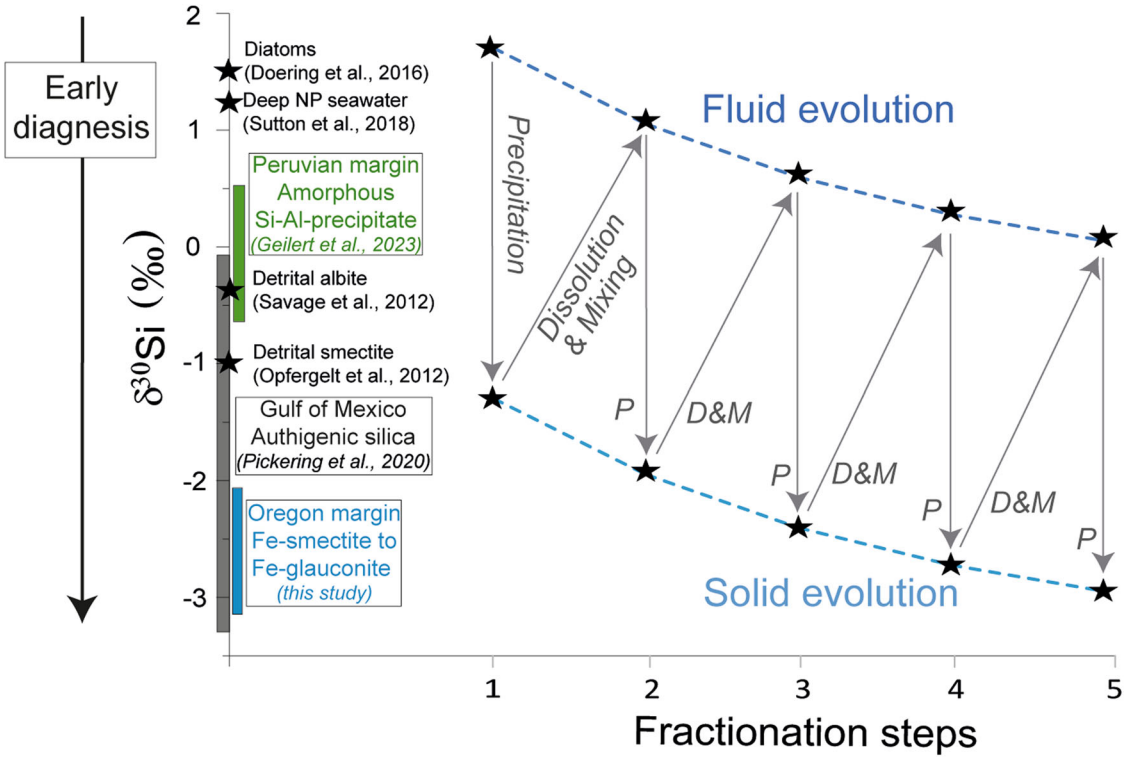

Fig. 4 | Modelled pore fluid and solid evolution as a function of clay maturation. Starting pore fluid composition was assumed to originate from a mixture of entrained deep North Pacific (NP) seawater (δ^{30}Si: 1.25‰[35]), as well as diatom (δ^{30}Si: 1.5‰[40]), detrital albite (δ^{30}Si: −0.4‰[41]), and detrital smectite (−1‰[42]) dissolution in the first step. Steps 2 to 5 have no contribution from diatom dissolution anymore but from pore fluid and authigenic clay dissolution from each previous step. Subsequent dissolution and reprecipitation shift δ^{30}Si to low values, attaining the lowest measured Oregon glauconite δ^{30}Si after five reaction steps (indicated as 1 to 5).

we suggest that the Si isotope shift documented here should be regarded as a minimum estimate. The usage of Si isotopes as silicate alteration tracers by looking at pore fluid shifts alone is problematic as the full extent of marine silicate alteration and associated marine alkalinity and cation cycling is likely masked and underestimated due to authigenic clay maturation.

In order to reliably interpret pore fluid δ^{30}Si signatures, clay maturity should be assessed using crystallographic and compositional indicators. If the authigenic clays are still in the early amorphous, gel-like stage, a direct correlation between pore fluid and precipitate δ^{30}Si appears to be feasible as the formation process can still be regarded as a uni-directional process, as the onset of multiple dissolution-reprecipitation steps has not yet begun. If the authigenic clays are already in a higher mature state, pore fluid δ^{30}Si has the potential to shift to lower values than seawater, mask the formation of authigenic clays and thus hamper the quantification of marine element budgets. Further studies are required to refine the early diagenetic impact on Si isotopes and validate a multi-proxy toolset to improve the assessment of marine element cycling.

Methods

Study site and sampling

The sediment core was collected via multi-corer deployment on the continental slope in 1200 m water depth in the eastern North Pacific on the Oregon margin (43°52' N, 124°54' W) in October 2012 (Fig. 1). A detailed description of the site characteristics and the sampling procedure is given in Abbott et al.[25].

EMP analyses and mineral mapping

Sediment aliquots from two depth intervals were selected (0–1.2 cm and 6.2–7.4 cm). The mineralogy of authigenic clay pellets and detrital feldspar grains suitable for in situ Si isotope analysis was determined by scanning electron microscope-energy dispersive X-ray spectroscopy (SEM-EDS) imaging and mineral mapping, using an FEI Teneo SEM running Thermo Fisher Maps Mineralogy[22]. Major and minor element composition of selected authigenic clay pellets and plagioclases was subsequently determined using a Cameca SX5 electron microprobe (EMP) (for details see Supplementary Method 2).

In situ Si isotope analyses

In situ silicon isotope ratios were measured by femtosecond laser ablation (fsLA) multi-collector inductively coupled plasma mass spectrometry (MC-ICP-MS) at the Helmholtz Laboratory for the Geochemistry of the Earth Surface (GFZ Potsdam). The method has been described in detail previously[38,39]. Samples and bracketing standard NBS28 were intensity matched by laser ablation frequency adjustments. Four reference materials were repeatedly analysed during the measurement sequence and are in good agreement with published values. See Supplementary Method 3 for more details.

Rayleigh model set-up

The model is based on an open system Rayleigh model following:

$$\delta^{30}Si_{pore\ fluid} = \delta^{30}Si_{initial} + \Delta^{30}Si * LN(f) \quad (1)$$

and

$$\delta^{30}Si_{solid} = \delta^{30}Si_{porefluid} + \Delta^{30}Si \quad (2)$$

We do not use the Rayleigh model in a classical sense, but assume a non-continuous, multistep precipitation from solution, in which each fraction is independent from the one before. This means, that $\delta^{30}Si_{initial}$ is calculated in each fractionation step independently. The $\delta^{30}Si_{initial}$ is the respective mixture between several components, with the components depending on the preceding fractionation step. In step 1, we assume a mixture of dissolving diatoms ($\delta^{30}Si$: 1.5[40]) contributing 70% and seawater

(δ^{30}Si: 1.25‰[35]), detrital albite (δ^{30}Si: −0.4‰[41]), and detrital clays (smectite with −1‰[42]), each contributing 10%. In model steps 2 to 5, we assume that the contribution from diatoms is negligible, because of the lowered solubility caused by the uptake of aluminium, that is released during detrital mineral dissolution[43]. Therefore, we assume a fluid mixture ($\delta^{30}Si_{initial}$ of steps 2 to 5), that is composed of the model results of the previous pore fluid (50%) and precipitating solid (20%) and a contribution (each 15%) from detrital albite (δ^{30}Si: −0.4‰[41]) and smectite (δ^{30}Si: −1‰[42]). The results are listed under column header 'Mixed initial fluid δ^{30}Si' in Supplementary Table 2.

The fraction remaining in solution (f) is kept constant at 0.8. Lower values of f cannot reproduce the low δ^{30}Si measured in the smectite-glauconites (Table 1). This finding also highlights, that dissolution is the dominating process and that a maximum of 20% ($1\text{-}f = 0.2$) is re-precipitating as higher mature clays. The best model fit is reached with a fractionation between solid and fluid ($\Delta^{30}Si$) of −3‰ (see model results for $\Delta^{30}Si$ of −2.5‰ and −2‰ in the Supplementary Method 1).

Data availability

Geochemical and Si isotope data is available in the main text and supplementary information of this publication.

Received: 14 March 2024; Accepted: 30 September 2024;
Published online: 09 October 2024

References

1. Wallmann, K. et al. Silicate weathering in anoxic marine sediments. *Geochim. Cosmochim. Acta* **72**, 2895–2918 (2008).
2. Wallmann, K., Geilert, S. & Scholz, F. Chemical Alteration of Riverine Particles in Seawater and Marine Sediments: Effects on Seawater Composition and Atmospheric CO2. *Am. J. Sci.* **7**, 1–39 (2023).
3. Krissansen-Totton, J. & Catling, D. C. Constraining climate sensitivity and continental versus seafloor weathering using an inverse geological carbon cycle model. *Nat. Commun.* **8**, 15423 (2017).
4. Isson, T. T. et al. Evolution of the Global Carbon Cycle and Climate Regulation on Earth Global Biogeochemical Cycles. *Global Biogeochem. Cycles* **34**, 1–28 (2020).
5. Torres, M. E. et al. Silicate weathering in anoxic marine sediment as a requirement for authigenic carbonate burial. *Earth-Science Rev*. **200**, 102960 (2020).
6. Baldermann, A. et al. The role of Fe on the formation and diagenesis of interstratified glauconite-smectite and illite-smectite: A case study of Lower Cretaceous shallow-water carbonates. *Chem. Geol.* **453**, 21–34 (2017).
7. Baldermann, A. et al. Impact of green clay authigenesis on element sequestration in marine settings. *Nat. Commun.* **13**, 1–11 (2022).
8. Gaudin, A. et al. Characterization and origin of Fe3+-montmorillonite in deep-water calcareous sediments (Pacific Ocean, Costa Rica Margin). *Clays Clay Miner* **53**, 452–465 (2005).
9. Mackenzie, F. T. & Garrels, R. M. Silicates: Reactivity with Sea Water. *Science (80-.)* **150**, 57–58 (1965).
10. Hong, W.-L., Torres, M. E. & Kutterolf, S. Towards a global quantification of volcanogenic aluminosilicate alteration rates through the mass balance of strontium in marine sediments. *Chem. Geol*. **550**, 119743 (2020).
11. Ward, J. P. J. et al. Stable silicon isotopes uncover a mineralogical control on the benthic silicon cycle in the Arctic Barents Sea. *Geochim. Cosmochim. Acta* **329**, 206–230 (2022).
12. Gaillardet, J., Dupre, B., Louvat, P. & Allegre, C. J. Global silicate weathering and CO_2 consumption rates deduced from the chemistry of large rivers. *Chem. Geol.* **159**, 3–30 (1999).
13. Gruber, C., Harlavan, Y., Pousty, D., Winkler, D. & Ganor, J. Enhanced chemical weathering of albite under seawater conditions and its potential effect on the Sr ocean budget. *Geochim. Cosmochim. Acta* **261**, 20–34 (2019).
14. Michalopoulos, P. & Aller, R. C. Rapid Clay Mineral Formation in Amazon Delta Sediments: Reverse Weathering and Oceanic Elemental Cycles. *Science (80)* **270**, 614–617 (1995).
15. Krissansen-Totton, J. & Catling, D. C. A coupled carbon-silicon cycle model over Earth history: Reverse weathering as a possible explanation of a warm mid-Proterozoic climate. *Earth Planet. Sci. Lett*. **537**, 116181 (2020).
16. Geilert, S. et al. Coastal El Niño triggers rapid marine silicate alteration on the seafloor. *Nat. Commun.* **14**, 1676 (2023).
17. Cassarino, L. et al. Sedimentary Nutrient Supply in Productive Hot Spots off the West Antarctic Peninsula Revealed by Silicon Isotopes. *Global Biogeochem. Cycles* **34**, e2019GB006486 (2020).
18. Luo, M. et al. Active Silica Diagenesis in the Deepest Hadal Trench Sediments. *Geophys. Res. Lett*. **49**, e2022GL099365 (2022).
19. Ehlert, C. et al. Stable silicon isotope signatures of marine pore waters – Biogenic opal dissolution versus authigenic clay mineral formation. *Geochim. Cosmochim. Acta* **191**, 102–117 (2016).
20. Abbott, A. N., Löhr, S. & Trethewy, M. Are Clay Minerals the Primary Control on the Oceanic Rare Earth Element Budget? *Front. Mar. Sci*. **6**, 504 (2019).
21. López-Quiros, A., Sánchez-Navas, A., Nieto, F. & Escutia, C. New insights into the nature of glauconite. *Am. Mineral.* **105**, 674–686 (2020).
22. Han, S. et al. Earth system science applications of next-generation SEM-EDS automated mineral mapping. *Front. Earth Sci*. **10**, 956912 (2022).
23. Pickering, R. A. et al. Using Stable Isotopes to Disentangle Marine Sedimentary Signals in Reactive Silicon Pools. *Geophys. Res. Lett.* **47**, 1–11 (2020).
24. Huang, T.-H. et al. Separating Si phases from diagenetically-modified sediments through sequential leaching. *Chem. Geol.* **637**, 121681 (2023).
25. Abbott, A. N., Haley, B. A., McManus, J. & Reimers, C. E. The sedimentary flux of dissolved rare earth elements to the ocean. *Geochim. Cosmochim. Acta* **154**, 186–200 (2015).
26. Meunier, A. & El Albani, A. The glauconite-Fe-illite-Fe-smectite problem: A critical review. *Terra Nov* **19**, 95–104 (2007).
27. Pringle, E. A. et al. Silicon isotopes reveal recycled altered oceanic crust in the mantle sources of Ocean Island Basalts. *Geochim. Cosmochim. Acta* **189**, 282–295 (2016).
28. Fernández-Landero, S. & Fernández-Caliani, J. C. Mineralogical and Crystal-Chemical Constraints on the Glauconite-Forming Process in Neogene Sediments of the Lower Guadalquivir Basin (SW Spain). *Minerals* **11**, 578 (2021).
29. Baldermann, A., Warr, L. N., Grathoff, G. H. & Dietzel, M. The rate and mechanism of deep-sea glauconite formation at the Ivory Coast - Ghana Marginal Ridge. *Clays Clay Miner* **61**, 258–276 (2013).
30. Odin, G. S. Matter, A. De glauconiarum origine. *Sedimentology* **28**, 611–641 (1981).
31. Bayon, G. et al. The silicon isotopic composition of fine-grained river sediments and its relation to climate and lithology. *Geochim. Cosmochim. Acta* **229**, 147–161 (2018).
32. Zhang, X. (Youn), Gaillardet, J., Barrier, L. & Bouchez, J. Li and Si isotopes reveal authigenic clay formation in a palaeo-delta. *Earth Planet. Sci. Lett.* **578**, 117339 (2022).
33. Geilert, S., Vroon, P. Z. & van Bergen, M. J. Effect of diagenetic phase transformation on the silicon isotope composition of opaline sinter deposits of Geysir, Iceland. *Chem. Geol.* **433**, 57–67 (2016).
34. Tatzel, M., von Blanckenburg, F., Oelze, M., Schuessler, J. A. & Bohrmann, G. The silicon isotope record of early silica diagenesis. *Earth Planet. Sci. Lett.* **428**, 293–303 (2015).
35. Sutton, J. N. et al. A Review of the Stable Isotope Bio-geochemistry of the Global Silicon Cycle and Its Associated Trace Elements. *Front. Earth Sci*. **5**, 112 (2018).
36. Liu, G. et al. Microbial reduction of Fe(III)-bearing clay minerals in the presence of humic acids. *Sci. Rep*. **7**, 45354 (2017).
37. Wheatcroft, R. A., Goñi, M. A., Richardson, K. N. & Borgeld, J. C. Natural and human impacts on centennial sediment accumulation

patterns on the Umpqua River margin, Oregon. *Mar. Geol.* **339**, 44–56 (2013).
38. Schuessler, J. A. & Von Blanckenburg, F. Testing the limits of micro-scale analyses of Si stable isotopes by femtosecond laser ablation multicollector inductively coupled plasma mass spectrometry with application to rock weathering. *Spectrochim. Acta - Part B At. Spectrosc* **98**, 1–18 (2014).
39. Geilert, S., Albers, E., Frick, D. A., Hansen, C. T. & von Blanckenburg, F. Systematic changes in serpentine Si isotope signatures across the Mariana forearc – a new proxy for slab dehydration processes. *Earth Planet. Sci. Lett*. **575**, 117193 (2021).
40. Doering, K. et al. Differences between mono-generic and mixed diatom silicon isotope compositions trace present and past nutrient utilisation off Peru. *Geochim. Cosmochim. Acta* **177**, 30–47 (2016).
41. Savage, P. S. et al. The silicon isotope composition of granites. *Geochim. Cosmochim. Acta* **92**, 184–202 (2012).
42. Opfergelt, S. et al. Silicon isotopes and the tracing of desilication in volcanic soil weathering sequences, Guadeloupe. *Chem. Geol.* **326–327**, 113–122 (2012).
43. Van Cappellen, P. & Qiu, L. Biogenic silica dissolution in sediments of the Southern Ocean. II Kinetics. *Deep. Res. II* **44**, 1129–1149 (1997).

Acknowledgements

We thank the GEOMAR early postdoctoral researcher program (to SG) and the Australian Research Council (Discovery Project DP210100462 'Glauconite: Archive Recording Timing and Triggers of Cambrian Radiation' to SCL), which supported this study. Oregon Margin sediments were collected by April Abbott through NSF Grant OCE-1147407 to Jim McManus and Brian Haley. No sampling permissions were required. The authors would like to thank the Helmholtz Laboratory for the Geochemistry of the Earth Surface (HELGES) for providing excellent (laboratory) infrastructure and in particular Josefine Holtz for her support during the fsLA-MC-ICP-MS measurements.

Author contributions

Sonja Geilert conceptualized the study, interpreted the measurement results and prepared the manuscript. Daniel A. Frick prepared and conducted the in situ Si isotope analyses. April N. Abbott coordinated the field work and processed the samples. Stefan C. Löhr conducted the mineral mapping and geochemical measurements. All authors contributed and commented on the manuscript.

Competing interests

The authors declare no competing interests.

Additional information

Supplementary information The online version contains supplementary material available at https://doi.org/10.1038/s43247-024-01746-4.

Correspondence and requests for materials should be addressed to Sonja Geilert.

Peer review information *Communications Earth & Environment* thanks Germain Bayon, Sophie Westacott and the other, anonymous, reviewer(s) for their contribution to the peer review of this work. Primary Handling Editors: Holly Stein and Carolina Ortiz Guerrero. A peer review file is available.